JACS
JOURNAL OF THE AMERICAN CHEMICAL SOCIETY
pubs.acs.org/JACS
Article

Divinylanthracene-Containing Tetracationic Organic Cyclophane with Near-Infrared Photoluminescence

Arthur H. G. David,[○] Amine Garci,[○] Seifallah Abid, Xuesong Li, Ryan M. Young,* James S. W. Seale, Jessica E. Hornick, Chandra S. Azad, Yang Jiao, Indranil Roy, Isil Akpinar, Tanay Kesharwani, Charlotte L. Stern, Michael R. Wasielewski,* and J. Fraser Stoddart*

Cite This: J. Am. Chem. Soc. 2023, 145, 9182–9190

ABSTRACT: Near-infrared (NIR) light is known to have outstanding optical penetration in biological tissues and to be non-invasive to cells compared with visible light. These characteristics make NIR-specific light optimal for numerous biological applications, such as the sensing of biomolecules or in theranostics. Over the years, significant progress has been achieved in the synthesis of fluorescent cyclophanes for sensing, bioimaging, and making optoelectronic materials. The preparation of NIR-emissive porphyrin-free cyclophanes is, however, still challenging. In an attempt for fluorescence emissions to reach into the NIR spectral region, employing organic tetracationic cyclophanes, we have inserted two 9,10-divinylanthracene units between two of the pyridinium units in cyclobis(paraquat-*p*-phenylene). Steady-state absorption, fluorescence, and transient-absorption spectroscopies reveal the deep-red and NIR photoluminescence of this cyclophane. This tetracationic cyclophane is highly soluble in water and has been employed successfully as a probe for live-cell imaging in a breast cancer cell line (MCF-7).

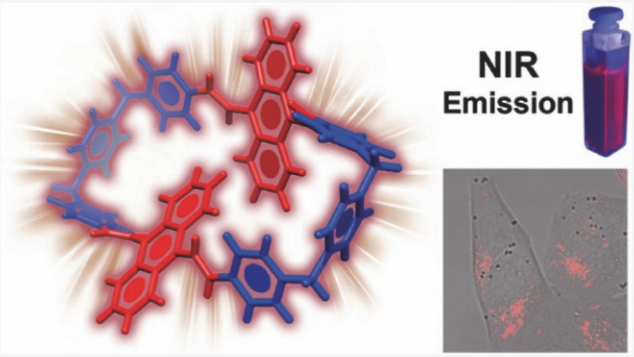

INTRODUCTION

Photoluminescent compounds and materials that emit in the near-infrared (NIR) range possess a deeper and much better optical penetration in biological tissues and are associated with less scattering and lower damage caused to the cells compared to the light emitted in the visible region of the spectrum. These properties render this class of fluorophores appealing candidates for various biological applications, such as biomolecular sensing,[1] bioimaging,[2] and theranostics.[3] In addition to these biomedical applications, NIR-emissive molecules can be incorporated[4] into high-performance, organic light-emitting diodes (OLEDs) and in the generation[5] of photonic devices.

Macrocycles bearing one or more aromatic rings embedded in their structures have also been called cyclophanes.[6] In the past half-century, numerous synthetic strategies to afford cyclophanes have been described in the literature[7] and have diversified substantially on account of their unique molecular recognition, which has attracted[8] much attention from supramolecular chemists. Among the wide variety of cyclophanes, those exhibiting additional fluorescence properties have emerged[9] as exceptional platforms for a myriad of applications, ranging from sensors[10] and bioimaging[11] to catalysis[12] and OLEDs.[13]

The vast majority of NIR-emissive macrocycles reported in the literature are porphyrins and their analogues[14] in addition to porphyrin-containing cyclophanes.[15] For example, Anderson and co-workers[15a−d,16] have developed a series of giant porphyrin-based NIR-emissive cyclophanes exhibiting emissions that can reach 1400 nm. The construction of NIR-emissive fluorescent porphyrin-free compounds, however, remains a challenge, despite the fact that a few examples, such as squaraine,[17] perylene diimide,[18] and π-extended anthracene-based[10c,19] cyclophanes, have been reported to exhibit these photoluminescent characteristics.

Recently, the insertion of various aromatic units into the structure of cyclobis(paraquat-*p*-phenylene)[20] (**CBPQT**$^{4+}$) has been investigated.[21] The aromatic units have been inserted both between two of the cyclophane's pyridinium units and on the bridges between the bipyridinium units, giving rise to the formation of cyclophanes capable of emitting blue[11a,22] (Figure 1a), green[23] (Figure 1b), yellow[11d,24] (Figure 1c), and

Received: February 2, 2023
Published: April 12, 2023

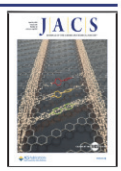

https://doi.org/10.1021/jacs.3c01244
J. Am. Chem. Soc. 2023, 145, 9182−9190

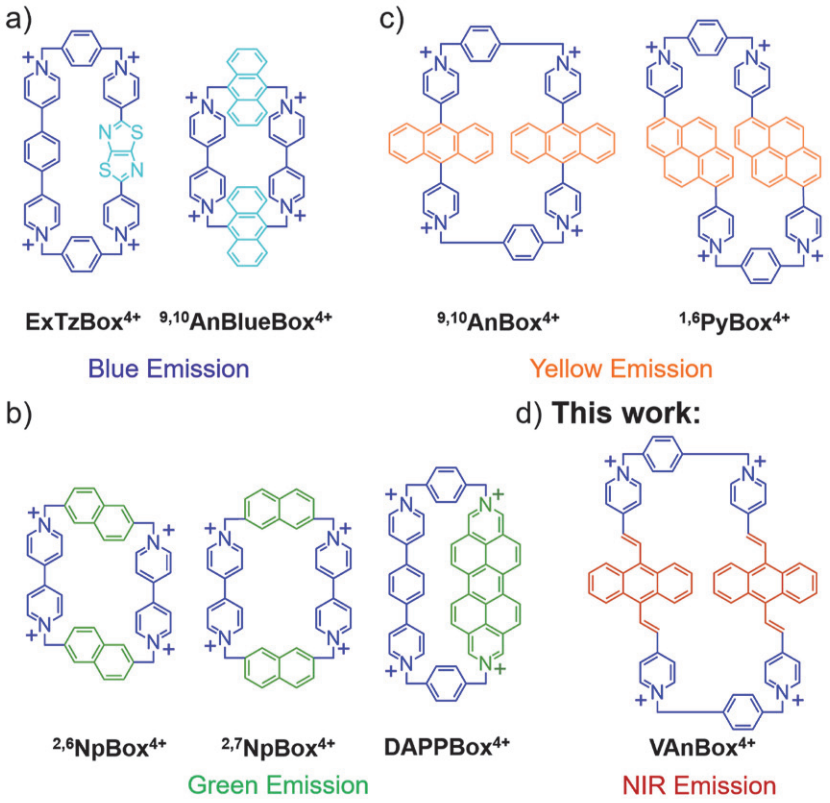

Figure 1. Structural formulas of related previously known photoluminescent **CBPQT**$^{4+}$-type cyclophanes with (a) blue fluorescence, e.g., **ExTzBox**$^{4+}$[11a] and **^{9,10}AnBlueBox**$^{4+}$;[22a] (b) green emission, e.g., **^{2,6}NpBox**$^{4+}$,[23b] **^{2,7}NpBox**$^{4+}$,[23b] and **DAPPBox**$^{4+}$;[23a] and (c) yellow luminescence, e.g., **^{9,10}AnBox**$^{4+}$,[11d] and **^{1,6}PyBox**$^{4+}$.[24a] (d) In this work, employing two 9,10-divinylanthracene units, the tetracationic cyclophane **VAnBox**$^{4+}$ emits NIR light, which was unattainable previously with the **CBPQT**$^{4+}$-type cyclophanes.

circularly polarized[25] light. In addition, one of the main advantages of these tetracationic cyclophanes is their high solubility in aqueous media, making it possible for them to address biological applications. Thus, both the blue-emissive **ExTzBox**$^{4+}$[11a] and the yellow-emissive **^{2,6}AnBox**$^{4+}$[11d] have been employed in live-cell imaging, and the extended **ExBox**$^{4+}$ has been utilized[26] as a drug delivery vehicle in photodynamic therapy. Although a variety of fluorescent **CBPQT**$^{4+}$-based cyclophanes have been designed, none of them exhibit fluorescence in the NIR spectral region. In this context, the development of NIR-emissive water-soluble organic **CBPQT**$^{4+}$-based cyclophanes presents a challenge of major importance when it comes to biotechnological applications.

The 9,10-divinylanthracene unit is a fluorophore, giving rise[10c,27] to NIR photoluminescence, which has been employed[10c,28] previously in the synthesis of self-assembled metal-based cyclophanes. In order to overcome the stability and lability issues characteristic of metallacycles, we report herein the design and synthesis of a 9,10-divinylanthracene-based organic tetracationic cyclophane (Figure 1d) whose fluorescence emission reaches into the NIR spectral region. This red-shifting of the photoluminescence of **VAnBox**$^{4+}$, compared to other synthetic tetracationic cyclophanes, and its excellent solubility in water[11a,d,24c,26] render it a good candidate as a NIR probe for live-cell imaging in a breast cancer cell line (MCF-7).

■ RESULTS AND DISCUSSION

Synthesis and Characterization. The syntheses of the model compound **2**·2PF$_6$ and the organic tetracationic cyclophane **VAnBox**·4PF$_6$ were performed (Scheme 1) using S$_N$2 reactions, a synthetic approach previously employed[20] for extended **CBPQT**$^{4+}$-based cyclophanes. Treatment of 9,10-bis[2-(4-pyridyl)vinyl]anthracene (**1**) with either benzyl bromide (BnBr) or α,α'-dibromo-*para*-xylene in MeCN afforded, respectively, the model compound **2**·2PF$_6$ and the intermediate **3**·2PF$_6$ in 35 and 76% yields after counterion exchange. The final macrocyclization between the bis-benzyl bromide **3**·2PF$_6$ and the bis-pyridine **1** in the presence of TBAI in MeCN at high dilution (0.17 mM) gave the desired organic tetracationic cyclophane **VAnBox**·4PF$_6$ in 19% yield after purification employing reverse-phase chromatography and counterion exchange to PF_6^-.

The cyclophane **VAnBox**·4PF$_6$ was characterized (Figures S5−S10) by 1D and 2D NMR spectroscopy. High-resolution mass spectrometry (HRMS) confirmed (Figure S12) the formation of **VAnBox**·4PF$_6$. The mass spectrum showed three characteristic peaks at m/z = 633.1896, 373.8053, and 244.1120, corresponding, respectively, to $[M - 2PF_6]^{2+}$, $[M - 3PF_6]^{3+}$, and $[M - 4PF_6]^{4+}$, whose experimental and theoretical isotopic distributions (Figures S13−S15) match well.

Single crystals of the model compound **2**·2PF$_6$ and the cyclophane **VAnBox**·4PF$_6$ were grown by slow evaporation of ^{i}PrOH in MeCN solutions of the compounds. The solid-state structure of **VAnBox**·4PF$_6$ (Figure 2a,b) shows that the size of the cyclophane is ca. 8.7 × 18.5 Å, and its bipyridinium pillars are bent and rather flexible. Unlike the previously investigated[11d] **^{9,10}AnBox**·4PF$_6$, the anthracene units of **VAnBox**·4PF$_6$ are not parallel. One of the anthracene units is directed

https://doi.org/10.1021/jacs.3c01244
J. Am. Chem. Soc. 2023, 145, 9182−9190

Scheme 1. Synthesis of a Model Compound 2·2PF$_6$ and the Cyclophane VAnBox·4PF$_6$ Employing S$_N$2 Reactions[a]

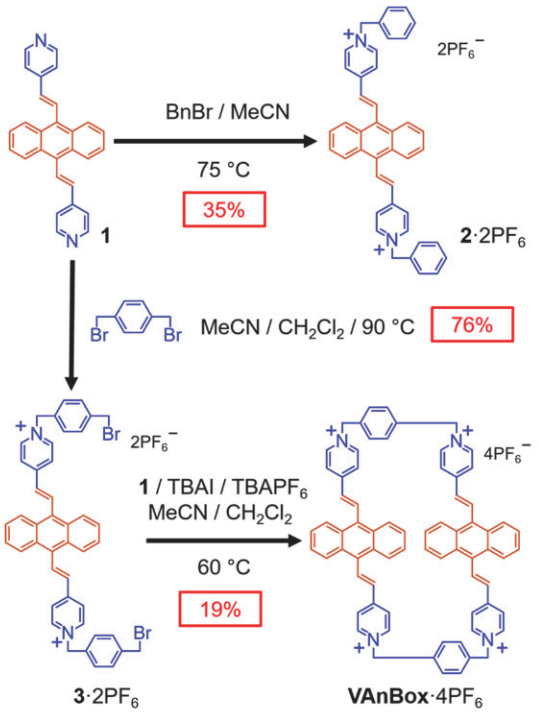

[a]The final macrocyclization was carried out at a concentration of 0.17 mM, affording the desired tetracationic cyclophane **VAnBox**·4PF$_6$ in 19% yield.

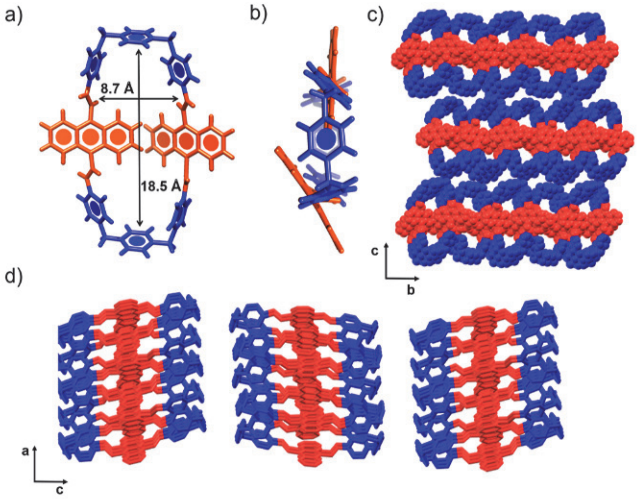

Figure 2. (a) Top-down view and (b) side-on view of the solid-state structure of **VAnBox**$^{4+}$. Illustration of the packing of **VAnBox**$^{4+}$ along the (c) *a*-axis and (d) *b*-axis, showing the tubular superstructure. Solvent molecules and PF_6^- anions were omitted for the sake of clarity.

toward the center of the cavity, obstructing it, while the other is pointing outside the cyclophane. The packing of **VAnBox**·4PF$_6$ displays (Figure 2c,d) tubular superstructures that are obstructed by anthracene units, forming crystalline nanotubes with two tunnels filled with PF_6^- anions and solvent molecules. In contrast, the solid-state structure (Figure S51) of the model compound **2**·2PF$_6$ does not adopt this superstructure on account of its constitutional linearity.

Optoelectronic Properties. In order to characterize the optoelectronic properties of the 9,10-divinylanthracene-based compounds, electrochemical experiments—namely cyclic voltammetry (CV) and differential pulse voltammetry (DPV)—were performed in MeCN solutions containing TBAPF$_6$ (0.1 M) as the supporting electrolyte. The CV of the cyclophane **VAnBox**$^{4+}$ and the model compound **2**$^{2+}$ exhibit (Figure 3a) one reduction wave (−0.46 and −0.48 V

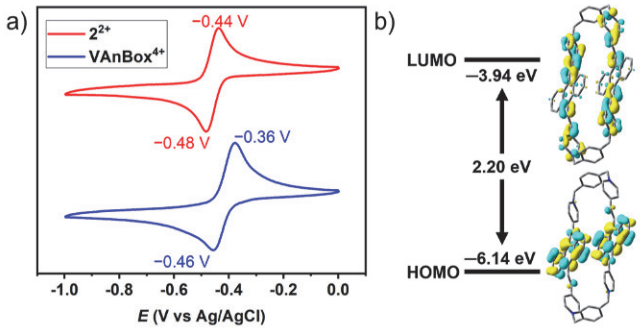

Figure 3. (a) CV data (scan rate: 200 mV s^{-1}) for **VAnBox**$^{4+}$ (blue trace) and the model compound **2**$^{2+}$ (red trace) in MeCN at concentrations of ca. 0.5 mM. The CV curve shows that both the model compound and the cyclophane undergo a single reversible reduction. (b) HOMO and LUMO energy levels of **VAnBox**$^{4+}$ visualized by DFT calculations, which possess a HOMO−LUMO gap of 2.20 eV, and their respective molecular orbitals. The HOMO and LUMO of the cyclophane show an intramolecular CT going from the anthracene to the pyridinium units.

vs Ag/AgCl, respectively, at a scan rate of 200 mV s^{-1}), corresponding to the reduction of the pyridinium (Py$^+$) units to their radical forms (Py$^\bullet$). The observation of a single reversible reduction of the pyridinium units indicates the absence of electronic communication between these units. The collected data allow the calculation of the HOMO−LUMO gap (Figure 3b) of the organic tetracationic cyclophane **VAnBox**$^{4+}$ to be 2.20 eV. In addition, density functional theory (DFT) calculations were performed, the results of which show that the molecular orbitals of the HOMO and LUMO energy levels of **VAnBox**$^{4+}$ are located (Figure 3b) on the anthracene and pyridinium units, respectively. Thus, these results demonstrate the potential for intramolecular charge transfer (CT) from the divinylanthracene core toward the pyridinium units.

The photophysical properties of the organic tetracationic cyclophane **VAnBox**·4PF$_6$ and the model compound **2**·2PF$_6$ were investigated. Both compounds exhibit (Figure 4a) similar UV−Vis spectra with several absorption bands between 200 and 350 nm and an additional CT band between 400 and 550 nm centered on 473 and 470 nm for **VAnBox**·4PF$_6$ and the model compound **2**·2PF$_6$, respectively, in MeCN. This behavior is typical[29] of Robin−Day class II mixed-valence systems. The molar extinction coefficients of **2**·2PF$_6$ and **VAnBox**·4PF$_6$ at their respective CT band maxima are 1.8×10^4 and 2.1×10^4 M^{-1} cm^{-1}. Remarkably, these values show only a modest increase in absorption for the cyclophane compared to the model compound, despite having twice the number of chromophores per molecule. Comparatively modest increases in extinction coefficient have been observed previously[30] in weakly coupled molecular dimers. This small increase, combined with the weak red shift in the CT absorption maximum, may be a consequence of the cyclophane

https://doi.org/10.1021/jacs.3c01244
J. Am. Chem. Soc. 2023, 145, 9182−9190

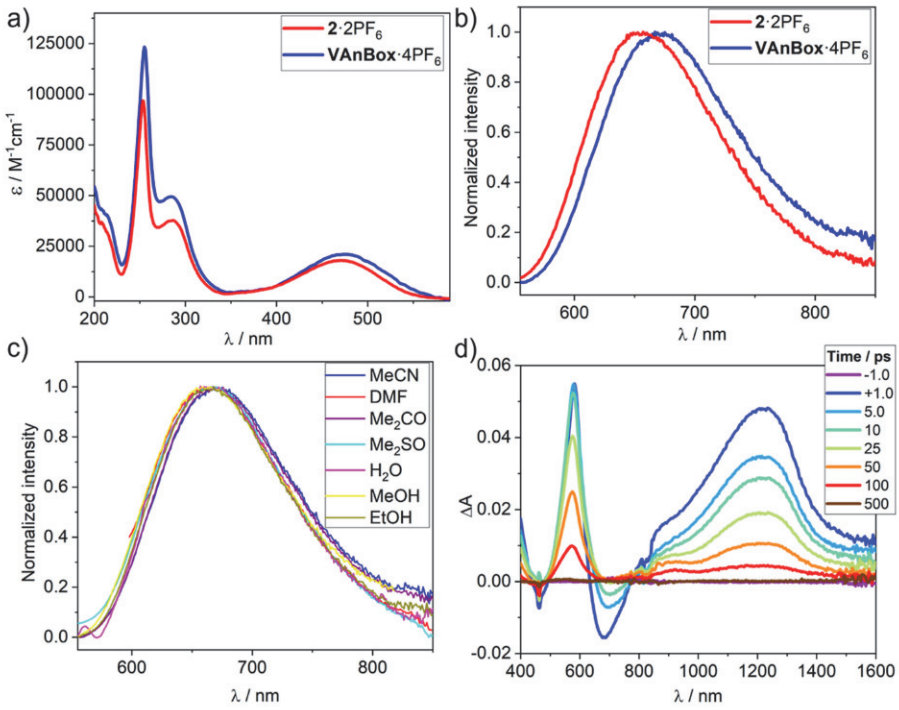

Figure 4. Photophysical properties of the model compound **2**·2PF$_6$ and the cyclophane **VAnBox**·4PF$_6$. UV−Vis (a) and normalized fluorescence (b) spectra of **2**·2PF$_6$ and **VAnBox**·4PF$_6$ in MeCN recorded at 20 °C at a concentration of ca. 1×10^{-5} M, except for the fluorescence spectrum of **VAnBox**·4PF$_6$ (ca. 6×10^{-6} M). In MeCN, both compounds exhibit a deep red/NIR photoluminescence and large Stokes shifts—5613 cm^{-1} for **2**·2PF$_6$ and 6149 cm^{-1} for **VAnBox**·4PF$_6$. (c) Normalized fluorescence spectra of **VAnBox**·4PF$_6$ in various solvents at ca. 6×10^{-6} M displaying similar spectra and an NIR emission in all solvents. (d) Transient absorption spectra of **VAnBox**·4PF$_6$ in MeCN following ∼100 fs excitation at 460 nm.

geometry: the CT transition dipole moments are oriented from the divinylanthracene core to each pyridinium unit, such that there are two opposing moments in **2**·2PF$_6$ with *J*-type coupling.[31] In the case of **VAnBox**·4PF$_6$, however, there are four of these transition moments, and the cyclophane geometry results in (Figure S31) four pairwise *J*-type versus two *H*-type couplings. Thus, the interference between these transition dipole moment couplings suppresses the total absorption and results in only a weak red shift (ca. 135 cm^{-1}) of the maximum. The broken symmetry suggested by the solid-state structure (Figure 2a) may also play a role in modulating the extinction coefficient through changes in effective conjugation lengths. The solid-state structures, however, represent the equilibrium states for the species in solution, where fluctuations and disorder will play a larger role.

The emission spectra in MeCN of these two compounds bearing 9,10-divinylanthracene units display (Figure 4b) a broad fluorescence band in the red and NIR spectral regions—from 550 to 850 nm—centered on 657 and 667 nm for **2**·2PF$_6$ and **VAnBox**·4PF$_6$, respectively. From the crossing of the (CT band-normalized) absorption and emission spectra (Figures S27,S29), the energy of the CT state is 2.22 and 2.16 eV in **2**·2PF$_6$ and **VAnBox**·4PF$_6$, respectively. These values are in good agreement with the electrochemical bandgap given above. Mulliken−Hush analysis[32] (Figure S30) shows that for the electronic coupling, the H_{DA} between the donor and acceptor units is similar for **2**·2PF$_6$ and **VAnBox**·4PF$_6$ at about 5280 and 5740 cm^{-1}, respectively, with the coupling strength tracking the change in the molar extinction coefficient.

On account of the high solubility of **VAnBox**$^{4+}$, the steady-state photophysical characterization was carried out (Table S1) in a variety of solvents, including H_2O as its chloride salt. The emission spectra (Figure 4c) of **VAnBox**$^{4+}$ in all solvents are very similar and show deep red and NIR photoluminescence. The quantum yields of emission for both compounds, in all the solvents investigated, are rather low, reaching values between 0.31 and 0.05%, depending on the solvent (Table S1). The NIR fluorescence of these compounds is, however, always detectable.

The excited-state dynamics of **2**·2PF$_6$ and **VAnBox**·4PF$_6$ in MeCN were explored using transient absorption spectroscopy by exciting the CT band at 460 nm. Figure 4d shows that upon excitation of **VAnBox**·4PF$_6$, ground-state bleaching at 460 nm as well as positive excited-state absorption (ESA) peaks at 367, 582, and 1218 nm appear. Stimulated emission at 680 nm is also present, which is consistent with the steady-state CT-based emission shown in Figure 2. The positive ESA features are attributed to the CT state between the anthracene donor and pyridinium acceptor groups, as suggested by the DFT results. All features decay within a nanosecond with minimal spectral evolution, with the exception of the stimulated emission feature, which shifts to an apparent minimum at 696 nm, then back to a minimum at 676 nm, with rate constants of $k_1 = (0.9 \pm 0.3\ \text{ps})^{-1}$ and $k_2 = (7.8 \pm 0.3\ \text{ps})^{-1}$, respectively, before ultimately decaying with a rate constant of $k_3 = (51.0 \pm 0.3\ \text{ps})^{-1}$. At later times during decay, the stimulated emission appears as an overall positive signal arising from the additive ESA features, although its shape remains as a distinctive depletion in the featureless absorption in that region. The kinetic analysis is presented in Figure S41. No triplets or other long-lived species are observed following the decay of the CT state.

https://doi.org/10.1021/jacs.3c01244
J. Am. Chem. Soc. 2023, 145, 9182−9190

Photoexcited **2**·2PF_6 shows similar behavior (Figure S40) with slight shifts compared to **VAnBox**·4PF_6, particularly in the stimulated emission band at 673 nm. This apparent minimum in **2**·2PF_6 shifts to 696 nm and then back to 677 nm with rate constants of k_1 = (4.4 ± 0.3 ps)$^{-1}$ and k_2 = (27 ± 1 ps)$^{-1}$, respectively. Following these shifts, the features decay together with k_1 = (79 ± 2 ps)$^{-1}$. Again, no long-lived species were observed.

The persistent presence of the stimulated emission throughout the entire lifetime of the excited state indicates that the emission is a result of radiative recombination (k_3) of the CT state. The distortion of the stimulated emission, relative to the steady-state emission, is caused by the overlapping positive ESA features that change the location of the apparent minimum. These ESA features evolve over time, first on the account of solvation within the first few ps and then through structural relaxation of the larger molecule. Solvation is faster in the cyclophane owing to the larger volume perturbing the solvation shell less severely; conversely, structural relaxation is restricted in the cyclophane as it is more rigid than in **2**·2PF_6 and does not permit slow, large amplitude nuclear motions. Additionally, the earliest spectral changes may arise from excited-state symmetry breaking within the acceptor−donor−acceptor system, where solvent or nuclear fluctuations force charge localization onto one side of the molecule.[33]

The short radiative recombination lifetimes are consistent with the low quantum yields of emission in these samples. The radiative and nonradiative decay rate contributions to the total observed rate constant k_3 (Table S2) show that the radiative component is the same (~50 ns) for **2**·2PF_6 and **VAnBox**·4PF_6 in MeCN, an observation which is consistent with their similar H_{DA} values. Thus, the nonradiative component (<100 ps) dominates, and the ratio of the rate constants k_3 between **2**·2PF_6 and **VAnBox**·4PF_6 is the same as the ratio of photoluminescence quantum yields. The (nonradiative) charge recombination of the CT state in **VAnBox**·4PF_6 is faster than in **2**·2PF_6 because of the lower CT-state energy of the cyclophane (2.16 vs 2.22 eV, respectively). Electron transfer to the ground state most likely resides in the Marcus-inverted region, such that the lower free-energy change results in a faster rate of CT.[34] The short CT lifetime precludes triplet formation as a result of radical pair intersystem crossing (RP-ISC) following radiative recombination. Indeed, the lack of observed triplets may suggest that, in solution, the dihedral angle between the divinylanthracene donor and the pyridinium acceptor is small, as a significant angle could induce triplet formation through spin−orbit charge-transfer ISC[35] (SOCT-ISC). The solid-state structure does show such a small angle for one side of the cyclophane, an observation which could imply that the excited-state symmetry-breaking immediately upon excitation favors structures with this geometry.

Live-Cell Imaging. The deep-red and NIR emissions of the divinylanthracene-based organic tetracationic cyclophane **VAnBox**·4Cl were exploited for live-cell imaging of a breast cancer cell line (MCF-7). The live-cell confocal microscopic images were taken following incubation with the cyclophane for 6 (Figure S54) and 24 h (Figures 5 and S53) at different micromolar concentrations. These confocal microscopic images display the emission of **VAnBox**·4Cl in the red channel (λ_{em} = 600−700 nm), which is clearly observable at a concentration of 1.0 μM (Figure 5c), very bright at 5.0 and 10.0 μM (Figure 5d,e) and not detected at 0.5 μM (Figure 5b)

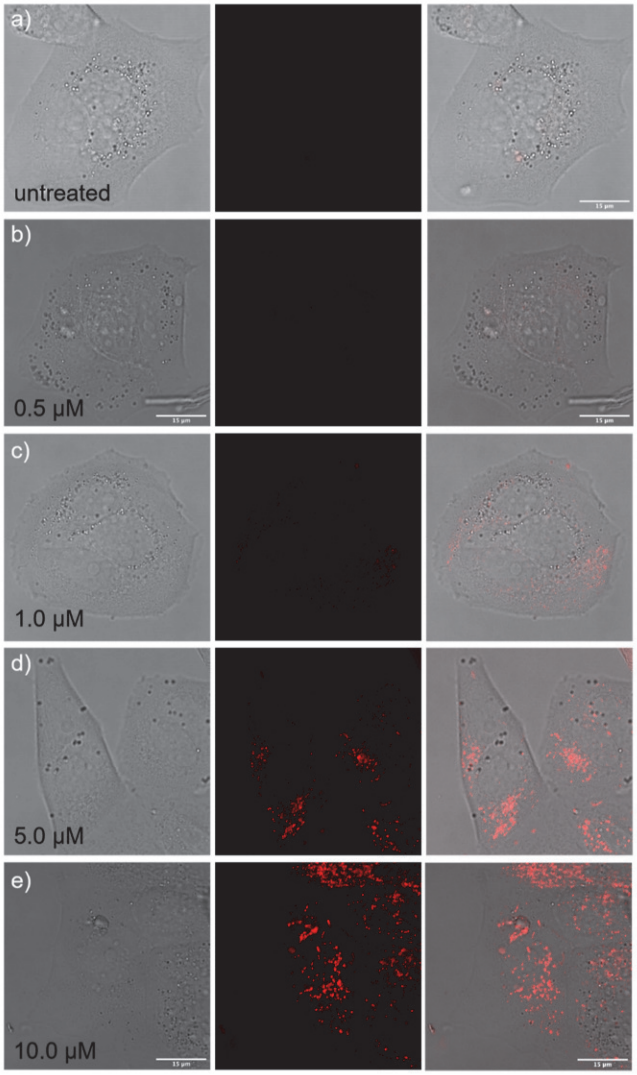

Figure 5. Live-cell confocal microscopy images of MCF-7 breast cancer cells. Cells were incubated for 24 h with **VAnBox**·4Cl at different concentrations: (b) 0.5 μM, (c) 1.0 μM, (d) 5.0 μM, (e) 10.0 μM, or (a) without the cyclophane, as a control experiment. Images of the cells show the transmitted light images (left), the emission of **VAnBox**·4Cl (middle, 600−700 nm), and the merged images (right). Scale bars are 15 μm. The cellular imaging experiment shows that the deep-red/NIR-emissive cyclophane **VAnBox**·4Cl is a suitable probe for bioimaging.

or in the absence (Figure 5a) of the cyclophane. These experiments show excellent cellular uptake after 6 and 24 h of incubation without significant differences in the brightness of **VAnBox**·4Cl in the cytoplasm. Furthermore, the **CBPQT**$^{4+}$-class of cyclophanes exhibit[11a,d] very low toxicity to living cells. In order to confirm this low cytotoxicity for **VAnBox**·4Cl, MCF-7 cells were stained with a LIVE/DEAD Fixable Violet Dead Cell Stain Kit prior to imaging. This cell viability experiment shows (Figure S55) that, even though some apoptosis occurs under all the treatment conditions, no significant cell death is observed after treatment with **VAnBox**·4Cl, even at a relatively high concentration (10 μM).

The divinylanthracene-containing cyclophane **VAnBox**·4Cl is, therefore, an excellent probe for live-cell imaging. On account of its NIR emission, biocompatibility, and cyclic structure, we envision that **VAnBox**·4Cl is a good candidate for

https://doi.org/10.1021/jacs.3c01244
J. Am. Chem. Soc. 2023, 145, 9182−9190

biomedical applications, such as drug delivery[36] and oxygen transport as endoperoxides for photoactivated therapy.[37]

CONCLUSIONS

In summary, we have designed and synthesized an organic tetracationic cyclophane by the insertion of a 9,10-divinylanthracene unit between the pyridinium rings of cyclobis(paraquat-*p*-phenylene). This cyclophane exhibits unique optoelectronic properties, including a CT-based photoluminescence in the NIR spectral region. This emissive cyclophane was applied to live-cell imaging, affording an intense emission in the red channel, while being nontoxic to the cells. The near-infrared fluorescence and the biocompatibility properties of this compound provide us with the incentive to employ this type of cyclophane in various biological applications ranging from drug delivery to theranostics.

ASSOCIATED CONTENT

Supporting Information

The Supporting Information is available free of charge at https://pubs.acs.org/doi/10.1021/jacs.3c01244.

Detailed methods, synthetic procedures, characterization data for all the compounds, including NMR, HRMS, UV−Vis, fluorescence, and TA spectra, computational methods, CV, X-ray crystallography, and cellular imaging (PDF)

Accession Codes

CCDC 2161001 and 2161003 contain the supplementary crystallographic data for this paper. These data can be obtained free of charge via www.ccdc.cam.ac.uk/data_request/cif, or by emailing data_request@ccdc.cam.ac.uk, or by contacting The Cambridge Crystallographic Data Centre, 12 Union Road, Cambridge CB2 1EZ, UK; fax: +44 1223 336033.

AUTHOR INFORMATION

Corresponding Authors

Ryan M. Young − *Department of Chemistry, Northwestern University, Evanston, Illinois 60208-3113, United States; Institute for Sustainability and Energy at Northwestern, Northwestern University, Evanston, Illinois 60208-3113, United States;* orcid.org/0000-0002-5108-0261; Email: ryan.young@northwestern.edu

Michael R. Wasielewski − *Department of Chemistry, Northwestern University, Evanston, Illinois 60208-3113, United States; Institute for Sustainability and Energy at Northwestern, Northwestern University, Evanston, Illinois 60208-3113, United States;* orcid.org/0000-0003-2920-5440; Email: m-wasielewski@northwestern.edu

J. Fraser Stoddart − *Department of Chemistry, Northwestern University, Evanston, Illinois 60208-3113, United States; School of Chemistry, University of New South Wales, Sydney, New South Wales 2052, Australia; Stoddart Institute of Molecular Science, Department of Chemistry, Zhejiang University, Hangzhou 310027, China; ZJU-Hangzhou Global Scientific and Technological Innovation Center, Hangzhou 311215, China;* orcid.org/0000-0003-3161-3697; Email: stoddart@northwestern.edu

Authors

Arthur H. G. David − *Department of Chemistry, Northwestern University, Evanston, Illinois 60208-3113, United States;* orcid.org/0000-0002-9275-2343

Amine Garci − *Department of Chemistry, Northwestern University, Evanston, Illinois 60208-3113, United States*

Seifallah Abid − *Department of Chemistry, Northwestern University, Evanston, Illinois 60208-3113, United States*

Xuesong Li − *Department of Chemistry, Northwestern University, Evanston, Illinois 60208-3113, United States;* orcid.org/0000-0002-2794-8390

James S. W. Seale − *Department of Chemistry, Northwestern University, Evanston, Illinois 60208-3113, United States;* orcid.org/0000-0001-8086-6020

Jessica E. Hornick − *Chemistry for Life Processes Institute and Department of Molecular Biosciences, Northwestern University, Evanston, Illinois 60208-3113, United States*

Chandra S. Azad − *Department of Chemistry, Northwestern University, Evanston, Illinois 60208-3113, United States;* orcid.org/0000-0003-2228-1600

Yang Jiao − *Department of Chemistry, Northwestern University, Evanston, Illinois 60208-3113, United States;* orcid.org/0000-0002-8437-0038

Indranil Roy − *Department of Chemistry, Northwestern University, Evanston, Illinois 60208-3113, United States;* orcid.org/0000-0003-3288-2207

Isil Akpinar − *Department of Chemistry, Northwestern University, Evanston, Illinois 60208-3113, United States*

Tanay Kesharwani − *Department of Chemistry, Northwestern University, Evanston, Illinois 60208-3113, United States; Department of Chemistry, University of West Florida, Pensacola, Florida 32514, United States;* orcid.org/0000-0001-8193-0004

Charlotte L. Stern − *Department of Chemistry, Northwestern University, Evanston, Illinois 60208-3113, United States;* orcid.org/0000-0002-9491-289X

Complete contact information is available at: https://pubs.acs.org/10.1021/jacs.3c01244

Author Contributions

○A.H.G.D. and A.G. contributed equally to this paper.

Notes

The authors declare no competing financial interest.

ACKNOWLEDGMENTS

The authors would like to thank Northwestern University (NU) for their continued support of this research. The authors acknowledge the Integrated Molecular Structure Education and Research Center (IMSERC) at NU and the Northwestern University Biological Imaging Facility (RRID: SCR_017767) for providing access to equipment for the experiments. The Biological Imaging Facility at Northwestern University is generously supported by the Chemistry for Life Processes Institute, the Department of Molecular Biosciences, the Rice Foundation, and the NU Office for Research. This project was also supported by the National Science Foundation under grant number DMR-2003739 (M.R.W. and R.M.Y.). This research used resources of the Advanced Photon Source, a U.S. Department of Energy (DOE) Office of Science User Facility operated for the DOE Office of Science by Argonne National Laboratory under contract no. DE-AC02-06CH11357. The use of the LS-CAT Sector 21 was supported by the Michigan Economic Development Corporation and the Michigan Technology Tri-Corridor (grant 085P1000817). J.S.W.S. gratefully acknowledges support from the Ryan Fellowship and the International Institute for Nanotechnology at North-

western University. The authors thank Paige J. Brown for her assistance on the fluorescence measurement.

REFERENCES

(1) (a) Kuba, M.; Kraus, T.; Pohl, R.; Hocek, M. Nucleotide-Bearing Benzylidene-Tetrahydroxanthylium Near-IR Fluorophore for Sensing DNA Replication, Secondary Structures and Interactions. *Chem.—Eur. J.* **2020**, *26*, 11950−11954. (b) Deng, H.; Liu, H.; Kang, W.; Lei, C.; Nie, Z.; Huang, Y.; Yao, S. Biomineralization Synthesis of a Near-Infrared Fluorescent Nanoprobe for Direct Glucose Sensing in Whole Blood. *Nanoscale* **2020**, *12*, 864−870. (c) Li, H.; Kim, H.; Xu, F.; Han, J.; Yao, Q.; Wang, J.; Pu, K.; Peng, X.; Yoon, J. Activity-Based NIR Fluorescent Probes Based on the Versatile Hemicyanine Scaffold: Design Strategy, Biomedical Applications, and Outlook. *Chem. Soc. Rev.* **2022**, *51*, 1795−1835.

(2) (a) Grimm, J. B.; Tkachuk, A. N.; Xie, L.; Choi, H.; Mohar, B.; Falco, N.; Schaefer, K.; Patel, R.; Zheng, Q.; Liu, Z.; Lippincott-Schwartz, J.; Brown, T. A.; Lavis, L. D. A General Method to Optimize and Functionalize Red-Shifted Rhodamine Dyes. *Nat. Methods* **2020**, *17*, 815−821. (b) Li, J.; Ma, Y.; Liu, S.; Mao, Z.; Chi, Z.; Qian, P.-C.; Wong, W.-Y. Soft Salts Based on Platinum(II) Complexes with High Emission Quantum Efficiencies in the Near Infrared Region for *in Vivo* Imaging. *Chem. Commun.* **2020**, *56*, 11681−11684. (c) Yang, S.; Tan, X.; Tang, L.; Yang, Q. Near-Infrared-II Bioimaging for *In Vivo* Quantitative Analysis. *Front. Chem.* **2021**, *9*, 76349. (d) Ding, F.; Feng, J.; Zhang, X.; Sun, J.; Fan, C.; Ge, Z. Responsive Optical Probes for Deep-Tissue Imaging: Photoacoustics and Second Near-Infrared Fluorescence. *Adv. Drug Deliv. Rev.* **2021**, *173*, 141−163. (e) Zhang, W.; Chen, S.; Sun, P.; Ye, S.; Fan, Q.; Song, J.; Zeng, P.; Qu, J.; Wong, W.-Y. NIR-II J-Aggregated Pt(II)-Porphyrin-Based Phosphorescent Probe for Tumor-Hypoxia Imaging. *Adv. Healthcare Mater.* **2022**, *11*, 2200467.

(3) (a) Chu, Y.; Shin, M. C.; Sung, J.; Park, J.; Kim, E.; Lee, S. Development of Theragnostic Tool Using NIR Fluorescence Probe Targeting Mitochondria in Glioma Cells. *Bioconjugate Chem.* **2019**, *30*, 1642−1648. (b) Laxman, K.; Reddy, B. P. K.; Mishra, S. K.; Robinson, A.; De, A.; Srivastava, R.; Ravikanth, M. Bioinspired Carrier-Free Peptide Conjugated BF_2-Oxasmaragdyrin Dye-Based Nano Self-Assemblies: A Photostable NIR Cancer Theragnostic Agent. *NPG Asia Mater.* **2020**, *12*, 75. (c) Laxman, K.; Reddy, B. P. K.; Mishra, S. K.; Gopal, M. B.; Robinson, A.; De, A.; Srivastava, R.; Ravikanth, M. BF_2-Oxasmaragdyrin Nanoparticles: A Non-Toxic, Photostable, Enhanced Non-Radiative Decay-Assisted Efficient Photothermal Cancer Theragnostic Agent. *ACS Appl. Mater. Interfaces* **2020**, *12*, 52329−52342.

(4) (a) Tuong Ly, K.; Chen-Cheng, R.-W.; Lin, H.-W.; Shiau, Y.-J.; Liu, S.-H.; Chou, P.-T.; Tsao, C.-S.; Huang, Y.-C.; Chi, Y. Near-Infrared Organic Light-Emitting Diodes with Very High External Quantum Efficiency and Radiance. *Nat. Photonics* **2017**, *11*, 63−68. (b) Zhang, Y.; Wang, Y.; Song, J.; Qu, J.; Li, B.; Zhu, W.; Wong, W.-Y. Near-Infrared Emitting Materials via Harvesting Triplet Excitons: Molecular Design, Properties, and Application in Organic Light Emitting Diodes. *Adv. Opt. Mater.* **2018**, *6*, 1800466. (c) Kim, D.-H.; D'Aléo, A.; Chen, X.-K.; Sandanayaka, A. D. S.; Yao, D.; Zhao, L.; Komino, T.; Zaborova, E.; Canard, G.; Tsuchiya, Y.; Choi, E.; Wu, J. W.; Fages, F.; Brédas, J.-L.; Ribierre, J.-C.; Adachi, C. High-Efficiency Electroluminescence and Amplified Spontaneous Emission from a Thermally Activated Delayed Fluorescent Near-Infrared Emitter. *Nat. Photonics* **2018**, *12*, 98−104. (d) Li, W.; Wang, B.; Miao, T.; Liu, J.; Lü, X.; Fu, G.; Shi, L.; Chen, Z.; Qian, P.; Wong, W.-Y. C_1-Symmetric $[Ir(C\hat{}N^1)(C\hat{}N^2)(O\hat{}O)]$-Tris-Heteroleptic Iridium(III)-Complexes with the Preferentially Horizontal Orientation for High-Performance Near-Infrared Organic Light-Emitting Diodes. *Adv. Opt. Mater.* **2021**, *9*, 2100117. (e) Zhang, H.; Chen, Z.; Zhu, L.; Wu, Y.; Xu, Y.; Chen, S.; Wong, W.-Y. High Performance NIR OLEDs with Emission Peak Beyond 760 nm and Maximum EQE of 6.39%. *Adv. Opt. Mater.* **2022**, *10*, 2200111.

(5) (a) Wang, Y.; Wu, H.; Li, P.; Chen, S.; Jones, L. O.; Mosquera, M. A.; Zhang, L.; Cai, K.; Chen, H.; Chen, X.-Y.; Stern, C. L.; Wasielewski, M. R.; Ratner, M. A.; Schatz, G. C.; Stoddart, J. F. Two-Photon Excited Deep-Red and Near-Infrared Emissive Organic Co-Crystals. *Nat. Commun.* **2020**, *11*, 4633. (b) Chen, X.; Li, Y.; Huang, K.; Huang, L.; Tian, X.; Dong, H.; Kang, R.; Hu, Y.; Nie, J.; Qiu, J.; Han, G. Trap Energy Upconversion-Like Near-Infrared to Near-Infrared Light Rejuvenateable Persistent Luminescence. *Adv. Mater.* **2021**, *33*, 2008722. (c) Zhang, J.; Ye, H.; Jin, Y.; Han, D. Recent Progress in Near-Infrared Organic Electroluminescent Materials. *Top. Curr. Chem.* **2022**, *380*, 6.

(6) (a) Vögtle, F. *Cyclophane Chemistry: Synthesis, Structures, and Reactions*; John Wiley & Sons: Chichester, 1993. (b) Liu, Z.; Nalluri, S. K. M.; Stoddart, J. F. Surveying Macrocyclic Chemistry: From Flexible Crown Ethers to Rigid Cyclophanes. *Chem. Soc. Rev.* **2017**, *46*, 2459−2478.

(7) (a) Cook, T. R.; Stang, P. J. Recent Developments in the Preparation and Chemistry of Metallacycles and Metallacages via Coordination. *Chem. Rev.* **2015**, *115*, 7001−7045. (b) Ogoshi, T.; Yamagishi, T. a.; Nakamoto, Y. Pillar-Shaped Macrocyclic Hosts Pillar[*n*]arenes: New Key Players for Supramolecular Chemistry. *Chem. Rev.* **2016**, *116*, 7937−8002. (c) Peng, S.; He, Q.; Vargas-Zúñiga, G. I.; Qin, L.; Hwang, I.; Kim, S. K.; Heo, N. J.; Lee, C.-H.; Dutta, R.; Sessler, J. L. Strapped Calix[4]pyrroles: From Syntheses to Applications. *Chem. Soc. Rev.* **2020**, *49*, 865−907. (d) Neira, I.; Blanco-Gómez, A.; Quintela, J. M.; García, M. D.; Peinador, C. Dissecting the "Blue Box": Self-Assembly Strategies for the Construction of Multipurpose Polycationic Cyclophanes. *Acc. Chem. Res.* **2020**, *53*, 2336−2346. (e) Li, Y.; Kono, H.; Maekawa, T.; Segawa, Y.; Yagi, A.; Itami, K. Chemical Synthesis of Carbon Nanorings and Nanobelts. *Acc. Mater. Res.* **2021**, *2*, 681−691.

(8) Steed, J. W.; Atwood, J. L. *Supramolecular Chemistry*, 3rd ed.; John Wiley & Sons: Chichester, 2022.

(9) Roy, I.; David, A. H. G.; Das, P. J.; Pe, D. J.; Stoddart, J. F. Fluorescent Cyclophanes and Their Applications. *Chem. Soc. Rev.* **2022**, *51*, 5557−5605.

(10) (a) Zapata, F.; Caballero, A.; White, N. G.; Claridge, T. D. W.; Costa, P. J.; Félix, V.; Beer, P. D. Fluorescent Charge-Assisted Halogen-Bonding Macrocyclic Halo-Imidazolium Receptors for Anion Recognition and Sensing in Aqueous Media. *J. Am. Chem. Soc.* **2012**, *134*, 11533−11541. (b) Shirinfar, B.; Ahmed, N.; Park, Y. S.; Cho, G.-S.; Youn, I. S.; Han, J.-K.; Nam, H. G.; Kim, K. S. Selective Fluorescent Detection of RNA in Living Cells by Using Imidazolium-Based Cyclophane. *J. Am. Chem. Soc.* **2013**, *135*, 90−93. (c) Li, Z.; Yan, X.; Huang, F.; Sepehrpour, H.; Stang, P. J. Near-Infrared Emissive Discrete Platinum(II) Metallacycles: Synthesis and Application in Ammonia Detection. *Org. Lett.* **2017**, *19*, 5728−5731. (d) Reiné, P.; Justicia, J.; Morcillo, S. P.; Abbate, S.; Vaz, B.; Ribagorda, M.; Orte, Á.; Álvarez de Cienfuegos, L.; Longhi, G.; Campaña, A. G.; Miguel, D.; Cuerva, J. M. Pyrene-Containing *ortho*-Oligo(phenylene)ethynylene Foldamer as a Ratiometric Probe Based on Circularly Polarized Luminescence. *J. Org. Chem.* **2018**, *83*, 4455−4463. (e) Agafontsev, A. M.; Shumilova, T. A.; Oshchepkov, A. S.; Hampel, F.; Kataev, E. A. Ratiometric Detection of ATP by Fluorescent Cyclophanes with Bellows-Type Sensing Mechanism. *Chem.—Eur. J.* **2020**, *26*, 9991−9997. (f) Dey, S.; Kumar, A.; Mondal, P. K.; Modi, K. M.; Chopra, D.; Jain, V. K. An Oxacalix[4]arene Derived Dual Sensing Fluorescent Probe for the Detection of As(V) and Cr(VI) Oxyanions in Aqueous Media. *Dalton Trans.* **2020**, *49*, 7459−7466.

(11) (a) Roy, I.; Bobbala, S.; Zhou, J.; Nguyen, M. T.; Nalluri, S. K. M.; Wu, Y.; Ferris, D. P.; Scott, E. A.; Wasielewski, M. R.; Stoddart, J. F. ExTzBox: A Glowing Cyclophane for Live-Cell Imaging. *J. Am. Chem. Soc.* **2018**, *140*, 7206−7212. (b) White, B. M.; Zhao, Y.; Kawashima, T. E.; Branchaud, B. P.; Pluth, M. D.; Jasti, R. Expanding the Chemical Space of Biocompatible Fluorophores: Nanohoops in Cells. *ACS Cent. Sci.* **2018**, *4*, 1173−1178. (c) Domarco, O.; Kieler, C.; Pirker, C.; Dinhof, C.; Englinger, B.; Reisecker, J. M.; Timelthaler, G.; García, M. D.; Peinador, C.; Keppler, B. K.; Berger, W.; Terenzi, A. Subcellular Duplex DNA and G-Quadruplex Interaction Profiling of a Hexagonal Pt^{II} Metallacycle. *Angew. Chem., Int. Ed.* **2019**, *58*,

https://doi.org/10.1021/jacs.3c01244
J. Am. Chem. Soc. 2023, 145, 9182−9190

8007−8012. (d) Garci, A.; Beldjoudi, Y.; Kodaimati, M. S.; Hornick, J. E.; Nguyen, M. T.; Cetin, M. M.; Stern, C. L.; Roy, I.; Weiss, E. A.; Stoddart, J. F. Mechanical-Bond-Induced Exciplex Fluorescence in an Anthracene-Based Homo[2]catenane. *J. Am. Chem. Soc.* **2020**, *142*, 7956−7967. (e) Lovell, T. C.; Bolton, S. G.; Kenison, J. P.; Shangguan, J.; Otteson, C. E.; Civitci, F.; Nan, X.; Pluth, M. D.; Jasti, R. Subcellular Targeted Nanohoop for One- and Two-Photon Live Cell Imaging. *ACS Nano* **2021**, *15*, 15285−15293. (f) Zeng, W.; Zhu, L.-Y.; Chen, Y.; Lin, M.-J. An AIE-Active Conjugated Macrocyclic Tetramaleimide for "Turn-On" Far Red/Near-Infrared Fluorescent Bioimaging. *Dyes Pigm.* **2021**, *190*, 109324.

(12) Li, Z.-B.; Lin, J.; Qin, Y.-C.; Pu, L. Enantioselective Fluorescent Recognition of a Soluble "Supported" Chiral Acid: Toward a New Method for Chiral Catalyst Screening. *Org. Lett.* **2005**, *7*, 3441−3444.

(13) (a) Yu, D.; Peng, T.; Zhang, H.; Bi, H.; Zhang, J.; Wang, Y. Basket-Shaped Quinacridone Cyclophanes: Synthesis, Solid-State Structures, and Properties. *New J. Chem.* **2010**, *34*, 2213−2219. (b) Chen, K.; Zhao, H.-R.; Fan, Z.-K.; Yin, G.; Chen, Q.-M.; Quan, Y.-W.; Li, S.-H.; Ye, S.-H. Macrospirocyclic Oligomer Based on Triphenylamine and Diphenylphosphine Oxide as a Bipolar Host for Efficient Blue Electrophosphorescent Organic Light-Emitting Diodes (OLEDs). *Org. Lett.* **2015**, *17*, 1413−1416. (c) Xue, J. Y.; Izumi, T.; Yoshii, A.; Ikemoto, K.; Koretsune, T.; Akashi, R.; Arita, R.; Taka, H.; Kita, H.; Sato, S.; Isobe, H. Aromatic Hydrocarbon Macrocycles for Highly Efficient Organic Light-Emitting Devices with Single-Layer Architectures. *Chem. Sci.* **2016**, *7*, 896−904. (d) Yoshii, A.; Ikemoto, K.; Izumi, T.; Taka, H.; Kita, H.; Sato, S.; Isobe, H. Periphery Design of Macrocyclic Materials for Organic Light-Emitting Devices with a Blue Phosphorescent Emitter. *Org. Lett.* **2019**, *21*, 2759−2762. (e) Izumi, S.; Higginbotham, H. F.; Nyga, A.; Stachelek, P.; Tohnai, N.; Silva, P. d.; Data, P.; Takeda, Y.; Minakata, S. Thermally Activated Delayed Fluorescent Donor−Acceptor−Donor−Acceptor π-Conjugated Macrocycle for Organic Light-Emitting Diodes. *J. Am. Chem. Soc.* **2020**, *142*, 1482−1491.

(14) (a) Gouterman, M.; Hanson, L. K.; Khalil, G.-E.; Leenstra, W. R.; Buchler, J. W. Porphyrins. XXXII. Absorptions and Luminescence of Cr(III) Complexes. *J. Chem. Phys.* **1975**, *62*, 2343−2353. (b) Ostrowski, J. C.; Susumu, K.; Robinson, M. R.; Therien, M. J.; Bazan, G. C. Near-Infrared Electroluminescent Light-Emitting Devices Based on Ethyne-Bridged Porphyrin Fluorophores. *Adv. Mater.* **2003**, *15*, 1296−1300. (c) Lim, J. M.; Shin, J.-Y.; Tanaka, Y.; Saito, S.; Osuka, A.; Kim, D. Protonated $[4n]\pi$ and $[4n+2]\pi$ Octaphyrins Choose Their Möbius/Hückel Aromatic Topology. *J. Am. Chem. Soc.* **2010**, *132*, 3105−3114. (d) Kim, T.; Duan, Z.; Talukdar, S.; Lei, C.; Kim, D.; Sessler, J. L.; Sarma, T. Excitonically Coupled Cyclic BF_2 Arrays of Calix[8]- and Calix[16]phyrin as Near-IR-Chromophores. *Angew. Chem., Int. Ed.* **2020**, *59*, 13063−13070.

(15) (a) O'Sullivan, M. C.; Sprafke, J. K.; Kondratuk, D. V.; Rinfray, C.; Claridge, T. D. W.; Saywell, A.; Blunt, M. O.; O'Shea, J. N.; Beton, P. H.; Malfois, M.; Anderson, H. L. Vernier Templating and Synthesis of a 12-Porphyrin Nano-Ring. *Nature* **2011**, *469*, 72−75. (b) Sprafke, J. K.; Kondratuk, D. V.; Wykes, M.; Thompson, A. L.; Hoffmann, M.; Drevinskas, R.; Chen, W.-H.; Yong, C. K.; Kärnbratt, J.; Bullock, J. E.; Malfois, M.; Wasielewski, M. R.; Albinsson, B.; Herz, L. M.; Zigmantas, D.; Beljonne, D.; Anderson, H. L. Belt-Shaped π-Systems: Relating Geometry to Electronic Structure in a Six-Porphyrin Nanoring. *J. Am. Chem. Soc.* **2011**, *133*, 17262−17273. (c) Liu, P.; Hisamune, Y.; Peeks, M. D.; Odell, B.; Gong, J. Q.; Herz, L. M.; Anderson, H. L. Synthesis of Five-Porphyrin Nanorings by Using Ferrocene and Corannulene Templates. *Angew. Chem., Int. Ed.* **2016**, *55*, 8358−8362. (d) Haver, R.; Tejerina, L.; Jiang, H.-W.; Rickhaus, M.; Jirasek, M.; Grübner, I.; Eggimann, H. J.; Herz, L. M.; Anderson, H. L. Tuning the Circumference of Six-Porphyrin Nanorings. *J. Am. Chem. Soc.* **2019**, *141*, 7965−7971. (e) Kaur, R.; Sen, S.; Larsen, M. C.; Tavares, L.; Kjelstrup-Hansen, J.; Ishida, M.; Zieleniewska, A.; Lynch, V. M.; Bähring, S.; Guldi, D. M.; Sessler, J. L.; Jana, A. Semiconducting Supramolecular Organic Frameworks Assembled from a Near-Infrared Fluorescent Macrocyclic Probe and Fullerenes. *J. Am. Chem. Soc.* **2020**, *142*, 11497−11505.

(16) Bols, P. S.; Anderson, H. L. Template-Directed Synthesis of Molecular Nanorings and Cages. *Acc. Chem. Res.* **2018**, *51*, 2083−2092.

(17) Brüning, C.; Welz, E.; Heilos, A.; Stehr, V.; Walter, C.; Engels, B.; Völker, S. F.; Lambert, C.; Engel, V. Macrocyclic *cis*-Indolenine Squaraine Dyes as Efficient Near Infrared Emitters. *J. Phys. Chem. C* **2015**, *119*, 6174−6180.

(18) Barendt, T. A.; Myers, W. K.; Cornes, S. P.; Lebedeva, M. A.; Porfyrakis, K.; Marques, I.; Félix, V.; Beer, P. D. The Green Box: An Electronically Versatile Perylene Diimide Macrocyclic Host for Fullerenes. *J. Am. Chem. Soc.* **2020**, *142*, 349−364.

(19) Miki, K.; Noda, T.; Gon, M.; Tanaka, K.; Chujo, Y.; Mizuhata, Y.; Tokitoh, N.; Ohe, K. Near-Infrared Circularly Polarized Luminescence Through Intramolecular Excimer Formation of Oligo(*p*-phenyleneethynylene)-Based Double Helicates. *Chem.−Eur. J.* **2019**, *25*, 9211−9216.

(20) Odell, B.; Reddington, M. V.; Slawin, A. M. Z.; Spencer, N.; Stoddart, J. F.; Williams, D. J. Cyclobis(paraquat-*p*-phenylene). A Tetracationic Multipurpose Receptor. *Angew Chem. Int. Ed. Engl.* **1988**, *27*, 1547−1550.

(21) (a) Ashton, P. R.; Ballardini, R.; Balzani, V.; Boyd, S. E.; Credi, A.; Gandolfi, M. T.; Gómez-López, M.; Iqbal, S.; Philp, D.; Preece, J. A.; Prodi, L.; Ricketts, H. G.; Stoddart, J. F.; Tolley, M. S.; Venturi, M.; Venturi, M.; White, A. J. P.; Williams, D. J. Simple Mechanical Molecular and Supramolecular Machines: Photochemical and Electrochemical Control of Switching Processes. *Chem.−Eur. J.* **1997**, *3*, 152−170. (b) Barnes, J. C.; Juríček, M.; Strutt, N. L.; Frasconi, M.; Sampath, S.; Giesener, M. A.; McGrier, P. L.; Bruns, C. J.; Stern, C. L.; Sarjeant, A. A.; Stoddart, J. F. ExBox: A Polycyclic Aromatic Hydrocarbon Scavenger. *J. Am. Chem. Soc.* **2013**, *135*, 183−192. (c) Barnes, J. C.; Juríček, M.; Vermeulen, N. A.; Dale, E. J.; Stoddart, J. F. Synthesis of Ex^{n}Box Cyclophanes. *J. Org. Chem.* **2013**, *78*, 11962−11969. (d) Dale, E. J.; Vermeulen, N. A.; Juríček, M.; Barnes, J. C.; Young, R. M.; Wasielewski, M. R.; Stoddart, J. F. Supramolecular Explorations: Exhibiting the Extent of Extended Cationic Cyclophanes. *Acc. Chem. Res.* **2016**, *49*, 262−273. (e) Chen, H.; Hou, S.; Wu, Q.; Jiang, F.; Zhou, P.; Zhang, L.; Jiao, Y.; Song, B.; Guo, Q.-H.; Chen, X.-Y.; Hong, W.; Lambert, C. J.; Stoddart, J. F. Promotion and Suppression of Single-Molecule Conductance by Quantum Interference in Macrocyclic Circuits. *Matter* **2021**, *4*, 3662−3676.

(22) (a) Neelakandan, P. P.; Sanju, K. S.; Ramaiah, D. Effect of Bridging Units on Photophysical and DNA Binding Properties of a Few Cyclophanes. *Photochem. Photobiol.* **2010**, *86*, 282−289. (b) Wu, H.; Chen, Y.; Zhang, L.; Anamimoghadam, O.; Shen, D.; Liu, Z.; Cai, K.; Pezzato, C.; Stern, C. L.; Liu, Y.; Stoddart, J. F. A Dynamic Tetracationic Macrocycle Exhibiting Photoswitchable Molecular Encapsulation. *J. Am. Chem. Soc.* **2019**, *141*, 1280−1289.

(23) (a) Gong, X.; Young, R. M.; Hartlieb, K. J.; Miller, C.; Wu, Y.; Xiao, H.; Li, P.; Hafezi, N.; Zhou, J.; Ma, L.; Cheng, T.; Goddard, W. A., III; Farha, O. K.; Hupp, J. T.; Wasielewski, M. R.; Stoddart, J. F. Intramolecular Energy and Electron Transfer within a Diazaperopyrenium-Based Cyclophane. *J. Am. Chem. Soc.* **2017**, *139*, 4107−4116. (b) Cetin, M. M.; Beldjoudi, Y.; Roy, I.; Anamimoghadam, O.; Bae, Y. J.; Young, R. M.; Krzyaniak, M. D.; Stern, C. L.; Philp, D.; Alsubaie, F. M.; Wasielewski, M. R.; Stoddart, J. F. Combining Intra- and Intermolecular Charge Transfer with Polycationic Cyclophanes to Design 2D Tessellations. *J. Am. Chem. Soc.* **2019**, *141*, 18727−18739. (c) Feng, Y.; Das, P. J.; Young, R. M.; Brown, P. J.; Hornick, J. E.; Weber, J. A.; Seale, J. S. W.; Stern, C. L.; Wasielewski, M. R.; Stoddart, J. F. Alkoxy-Substituted Quadrupolar Fluorescent Dyes. *J. Am. Chem. Soc.* **2022**, *144*, 16841−16854.

(24) (a) Garci, A.; Weber, J. A.; Young, R. M.; Kazem-Rostami, M.; Ovalle, M.; Beldjoudi, Y.; Atilgan, A.; Bae, Y. J.; Liu, W.; Jones, L. O.; Stern, C. L.; Schatz, G. C.; Farha, O. K.; Wasielewski, M. R.; Fraser Stoddart, J. Mechanically Interlocked Pyrene-Based Photocatalysts. *Nat. Catal.* **2022**, *5*, 524−533. (b) Garci, A.; David, A. H. G.; Le Bras, L.; Ovalle, M.; Abid, S.; Young, R. M.; Liu, W.; Azad, C. S.; Brown, P. J.; Wasielewski, M. R.; Fraser Stoddart, J. Thermally Controlled

https://doi.org/10.1021/jacs.3c01244
J. Am. Chem. Soc. 2023, 145, 9182−9190

Exciplex Fluorescence in a Dynamic Homo[2]catenane. *J. Am. Chem. Soc.* **2022**, *144*, 23551−23559. (c) Zheng, X.; Lei, S.-N.; Gao, Z.; Dong, X.; Xiao, H.; Liu, W.; Tung, C.-H.; Wu, L.-Z.; Wang, P.; Cong, H. Supramolecular Photosensitizers Using Extended Macrocyclic Hosts for Photodynamic Therapy with Distinct Cellular Delivery. *Chem. Sci.* **2023**, *14*, 3523−3530.

(25) Garci, A.; Abid, S.; David, A. H. G.; Codesal, M. D.; Đorđević, L.; Young, R. M.; Sai, H.; Le Bras, L.; Perrier, A.; Ovalle, M.; Brown, P. J.; Stern, C. L.; Campaña, A. G.; Stupp, S. I.; Wasielewski, M. R.; Blanco, V.; Stoddart, J. F. Aggregation Induced Emission and Circularly Polarized Luminescence Duality in Tetracationic Binaphthyl-Based Cyclophanes. *Angew. Chem., Int. Ed.* **2022**, *61*, No. e202208679.

(26) Roy, I.; Bobbala, S.; Young, R. M.; Beldjoudi, Y.; Nguyen, M. T.; Cetin, M. M.; Cooper, J. A.; Allen, S.; Anamimoghadam, O.; Scott, E. A.; Wasielewski, M. R.; Stoddart, J. F. A Supramolecular Approach for Modulated Photoprotection, Lysosomal Delivery, and Photodynamic Activity of a Photosensitizer. *J. Am. Chem. Soc.* **2019**, *141*, 12296−12304.

(27) (a) Chen, X.-M.; Chen, Y.; Yu, Q.; Gu, B.-H.; Liu, Y. Supramolecular Assemblies with Near-Infrared Emission Mediated in Two Stages by Cucurbituril and Amphiphilic Calixarene for Lysosome-Targeted Cell Imaging. *Angew. Chem., Int. Ed.* **2018**, *57*, 12519−12523. (b) Yin, W.; Meng, L.; Yu, T.; Chen, J.; Hu, R.; Yang, G.; Zeng, Y.; Li, Y. Crystallization and Near-Infrared Emission from Host−Guest Based Supramolecular Polymers. *New J. Chem.* **2021**, *45*, 9761−9765.

(28) (a) Chowdhury, A.; Howlader, P.; Mukherjee, P. S. Aggregation-Induced Emission of Platinum(II) Metallacycles and Their Ability to Detect Nitroaromatics. *Chem.−Eur. J.* **2016**, *22*, 7468−7478. (b) Shan, W.-L.; Gao, W.-X.; Lin, Y.-J.; Jin, G.-X. Light-Initiated Reversible Conversion of Macrocyclic Endoperoxides Derived from Half-Sandwich Rhodium-Based Metallarectangles. *Dalton Trans.* **2018**, *47*, 2769−2777.

(29) Robin, M. B.; Day, P. Mixed Valence Chemistry−A Survey and Classification. *Adv. Inorg. Chem. Radiochem.* **1968**, *10*, 247−422.

(30) (a) Zirzlmeier, J.; Lehnherr, D.; Coto, P. B.; Chernick, E. T.; Casillas, R.; Basel, B. S.; Thoss, M.; Tykwinski, R. R.; Guldi, D. M. Singlet Fission in Pentacene Dimers. *Proc. Natl. Acad. Sci. U.S.A.* **2015**, *112*, 5325−5330. (b) Basel, B. S.; Zirzlmeier, J.; Hetzer, C.; Reddy, S. R.; Phelan, B. T.; Krzyaniak, M. D.; Volland, M. K.; Coto, P. B.; Young, R. M.; Clark, T.; Thoss, M.; Tykwinski, R. R.; Wasielewski, M. R.; Guldi, D. M. Evidence for Charge-Transfer Mediation in the Primary Events of Singlet Fission in a Weakly Coupled Pentacene Dimer. *Chem* **2018**, *4*, 1092−1111.

(31) (a) Kasha, M.; Rawls, H. R.; Ashraf El-Bayoumi, M. The Exciton Model in Molecular Spectroscopy. *Pure Appl. Chem.* **1965**, *11*, 371−392. (b) Hestand, N. J.; Spano, F. C. Expanded Theory of *H*- and *J*-Molecular Aggregates: The Effects of Vibronic Coupling and Intermolecular Charge Transfer. *Chem. Rev.* **2018**, *118*, 7069−7163.

(32) Brunschwig, B. S.; Creutz, C.; Sutin, N. Optical Transitions of Symmetrical Mixed-Valence Systems in the Class II−III Transition Regime. *Chem. Soc. Rev.* **2002**, *31*, 168−184.

(33) Vauthey, E. Photoinduced Symmetry-Breaking Charge Separation. *ChemPhysChem* **2012**, *13*, 2001−2011.

(34) Marcus, R. A. On the Theory of Oxidation−Reduction Reactions Involving Electron Transfer. I. *J. Chem. Phys.* **1956**, *24*, 966−978.

(35) (a) El-Sayed, M. A. Effect of Spin Orbit Interactions on the Dipolar Nature of the Radiative Microwave Zero-Field Transitions in Aromatic Molecules. *J. Chem. Phys.* **1974**, *60*, 4502−4507. (b) Colvin, M. T.; Ricks, A. B.; Scott, A. M.; Co, D. T.; Wasielewski, M. R. Intersystem Crossing Involving Strongly Spin Exchange-Coupled Radical Ion Pairs in Donor−Bridge−Acceptor Molecules. *J. Phys. Chem. A* **2012**, *116*, 1923−1930. (c) Dong, Y.; Sukhanov, A. A.; Zhao, J.; Elmali, A.; Li, X.; Dick, B.; Karatay, A.; Voronkova, V. K. Spin−Orbit Charge-Transfer Intersystem Crossing (SOCT-ISC) in Bodipy-Phenoxazine Dyads: Effect of Chromophore Orientation and Conformation Restriction on the Photophysical Properties. *J. Phys. Chem. C* **2019**, *123*, 22793−22811.

(36) (a) Zhang, J.; Ma, P. X. Cyclodextrin-Based Supramolecular Systems for Drug Delivery: Recent Progress and Future Perspective. *Adv. Drug Delivery Rev.* **2013**, *65*, 1215−1233. (b) Plesselova, S.; Garcia-Cerezo, P.; Blanco, V.; Reche-Perez, F. J.; Hernandez-Mateo, F.; Santoyo-Gonzalez, F.; Giron-Gonzalez, M. D.; Salto-Gonzalez, R. Polyethylenimine−Bisphosphonate−Cyclodextrin Ternary Conjugates: Supramolecular Systems for the Delivery of Antineoplastic Drugs. *J. Med. Chem.* **2021**, *64*, 12245−12260.

(37) Kuang, S.; Wei, F.; Karges, J.; Ke, L.; Xiong, K.; Liao, X.; Gasser, G.; Ji, L.; Chao, H. Photodecaging of a Mitochondria-Localized Iridium(III) Endoperoxide Complex for Two-Photon Photoactivated Therapy under Hypoxia. *J. Am. Chem. Soc.* **2022**, *144*, 4091−4101.

https://doi.org/10.1021/jacs.3c01244
J. Am. Chem. Soc. 2023, 145, 9182−9190